# Performance of Coded Offset Quadrature Phase-Shift Keying (OQPSK) and MIL-STD Shaped OQPSK (SOQPSK) with Iterative Decoding

L. Li[1] and M. K. Simon[1]

*We show that, similar to the trellis-coded modulation representation of MIL-STD shaped offset quadrature phase-shift keying (SOQPSK), offset quadrature phase-shift keying (OQPSK) can be decomposed into a "degraded" trellis encoder and a memoryless mapper. Based on the representations of OQPSK and MIL-STD SOQPSK as trellis-coded modulations, we investigate the potential coding gains achievable from the application of simple outer codes to form a concatenated coding structure with iterative decoding. For MIL-STD SOQPSK, we describe the optimum receiver corresponding to its trellis-coded modulation form and then propose a simplified receiver. The bit-error-rate (BER) performances of both receivers for uncoded and coded MIL-STD SOQPSK are simulated and compared to those of OQPSK and Feher-patented quadrature phase-shift keying (FQPSK). The asymptotic BER performance of MIL-STD SOQPSK also is analyzed and compared to that of OQPSK and FQPSK. Simulation results show that, compared to their uncoded systems, both OQPSK and MIL-STD SOQPSK obtain significant coding gains by applying iterative decoding to either the parallel concatenated coding scheme or the serial one, even when very simple outer codes are used.*

## I. Introduction

Offset quadrature phase-shift keying (OQPSK) is a constant-envelope modulation that has no 180-deg phase shifts and, therefore, has a much higher spectral containment than non-offset quadrature phase-shift keying (QPSK) when transmitted over band-limited nonlinear channels. To further bandlimit an OQPSK signal, shaped OQPSK (SOQPSK) was introduced in [1], and its initial version was referred to as MIL-STD SOQPSK after it was adopted as part of a military standard. The frequency-shaping pulse for MIL-STD SOQPSK in its continuous phase modulation (CPM) representation is rectangular, and it lasts one bit interval. Later on more spectrally efficient versions of SOQPSK were developed in [2,3], and

[1] Communications Systems and Research Section.

The research described in this publication was carried out by the Jet Propulsion Laboratory, California Institute of Technology, under a contract with the National Aeronautics and Space Administration.

these variants are comparable to or even better than Feher-patented QPSK (FQPSK) [4] with regard to spectral and/or power efficiency [2,3,5,6].[2]

In a previous article [7], we introduced a cross-correlated trellis-coded quadrature modulation (XTCQM) representation for MIL-STD SOQPSK. XTCQM is a generic modulation scheme containing both memory and cross-correlation between the in-phase (I) and quadrature-phase (Q) channels [8]. In addition to MIL-STD SOQPSK, another specific embodiment of XTCQM is FQPSK [9–13]. Like FQPSK, the representation of MIL-STD SOQPSK in the form of XTCQM allows identification of an optimum receiver for it and allows for its inherent memory to be used in the iterative decoding of its coded systems. In this article, we describe such an optimum receiver and investigate the potential improvement in power efficiency obtained from exploring the inherent memory of MIL-STD SOQPSK in a coded system with iterative decoding. Furthermore, we introduce a representation for OQPSK similar to that of XTCQM for MIL-STD SOQPSK. Based on this representation of OQPSK and the XTCQM representation of MIL-STD SOQPSK, we present a symbol-by-symbol mapping for both OQPSK and MIL-STD SOQPSK that is performed directly on the input I and Q data sequences in every symbol (2-bit) interval. This direct symbol-by-symbol mapping results in a clear interpretation of MIL-STD SOQPSK as being composed of a cross-correlated trellis encoder and a memoryless mapper, and of OQPSK as being composed of a "degraded" trellis encoder and a memoryless mapper. Such decomposition of OQPSK makes it possible to apply iterative decoding to coded OQPSK, where the degraded trellis code of OQPSK, after being remapped to its recursive version, can be viewed as an inner code of a concatenated coding structure. Note that, previous to this article, the application of iterative demodulation and decoding to phase-shift keying (PSK) schemes has been considered only for coded differential phase-shift keying (DPSK) and differential QPSK (DQPSK) [14–16]. The performance of coded OQPSK with iterative decoding provides a lower bound to that of coded MIL-STD SOQPSK and FQPSK.

In an effort to reduce receiver complexity while maintaining reasonable performance, we also propose a simplified receiver for MIL-STD SOQPSK. This simplified receiver requires only half of the matched filters used in the optimum receiver, and it has the same complexity as the simplified receiver for FQPSK [17]. We then simulate the bit-error-rate (BER) performances of the optimum receiver and the simplified receiver for uncoded and coded MIL-STD SOQPSK and compare them to those of OQPSK and FQPSK. In the coded case, we investigate the serial concatenated system with two very simple codes of different rates as outer codes and the parallel concatenated (turbo-like) system without any outer codes. Simulation results show that, compared to the uncoded case, there are significant coding gains for both parallel and serial concatenated systems even with these simple codes.

## II. Decomposition of OQPSK

In [7] we described an 8-state bit-interval trellis diagram of OQPSK based on its CPM representation. In order to show the time-invariant symbol-interval trellis representation of OQPSK and the corresponding equivalent transmitter implementation of OQPSK, we first give a brief review of the CPM representation of OQPSK.

### A. The CPM Representation of OQPSK

It is known that a conventional OQPSK signal can be represented as a CPM signal in the form of [18]

$$s(t) = \sqrt{\frac{2E_b}{T_b}} \cos\big(2\pi f_c t + \phi(t, \boldsymbol{\alpha}) + \phi_0\big), \quad nT_b \le t \le (n+1)T_b$$

where $E_b$ and $T_b$ denote the energy and duration of a bit, respectively, $f_c$ is the carrier frequency, and $\phi_0$ is an arbitrary phase constant that, without loss of generality, can be set to zero. In addition, $\phi(t, \boldsymbol{\alpha})$ is the phase modulation process that can be expressed as

[2] Note that MIL-STD SOQPSK and its variants are unlicensed technologies.

$$\phi(t, \boldsymbol{\alpha}) = 2\pi \sum_{i \le n} \alpha_i h q(t - iT_b)$$

where, for OQPSK, the modulation index $h = 1/2$, the normalized phase pulse $q(t)$ is a step function (equivalently, the frequency pulse $g(t) = dq(t)/dt$ is a delta function, i.e., $g(t) = (1/2)\delta(t)$), and the $i$th element of the effective data sequence $\boldsymbol{\alpha} = (\cdots, \alpha_{-2}, \alpha_{-1}, \alpha_0, \alpha_1, \alpha_2, \cdots)$, $\alpha_i$, is related to the true input binary ($\pm 1$) data sequence $\mathbf{a} = (\cdots, a_{-2}, a_{-1}, a_0, a_1, a_2, \cdots)$ by [18]

$$\alpha_i = (-1)^{i+1} \frac{a_{i-1}(a_i - a_{i-2})}{2} \tag{1}$$

Detailed explanations on how Eq. (1) can be obtained through an 8-state (3-bit-state) trellis diagram of OQPSK are given by the authors in [7]. Note that for this 3-bit trellis state variable, the first bit defines whether the coming input bit $a_i$ corresponds to an even interval (I) or an odd interval (Q), while the remaining two bits represent the current phase state, assuming the four phase states $\pi/4, 3\pi/4, 5\pi/4, 7\pi/4$ are assigned the bit mappings (in the form of "IQ" bits) 00, 10, 11, 01, respectively. As shown in Fig. 2 of [7], in each bit (half-symbol) interval this 8-state trellis diagram of OQPSK gives the corresponding $\alpha_i$ for an input bit $a_i$ associated with the transition between a pair of states. Based on this trellis diagram, in the following subsection we consider transitions between the four phase states corresponding to a pair of input bits in each symbol interval.

### B. A Time-Invariant Symbol-Interval Trellis Representation of OQPSK

Without loss of generality, assume that in each symbol interval the first bit of the input pair is always an I bit. Then, given the 8-state trellis diagram of OQPSK in Fig. 2 of [7], we can easily obtain the trellis between the four phase states $(\pi/4)(00)$, $(3\pi/4)(10)$, $(5\pi/4)(11)$, $(7\pi/4)(01)$, which is illustrated in Fig. 1. Note that we have drawn the trellis in expanded form with each transition interval (now 2 bits in duration) showing the transitions leaving from one of the four phase states. In Fig. 1, each branch is now labeled with a pair of output $\alpha$ values, i.e., $\alpha_i, \alpha_{i+1}$. The corresponding pair of input bits is the same as the pair of bits representing the terminating phase state. Given the pair of outputs $(\alpha_i, \alpha_{i+1})$, for each transition there is a pair of waveforms $\big(s_I(t) = \cos[\phi(t, \alpha_i, \alpha_{i+1}) + \phi_0], s_Q(t) = \sin[\phi(t, \alpha_i, \alpha_{i+1}) + \phi_0]\big)$ associated with it, which represents the pair of symbols synchronously transmitted on the I and Q channels. Here $\phi_0$ is the initial phase of each transition indicated by the starting phase state, and in each symbol interval

$$\phi(t, \alpha_i, \alpha_{i+1}) = \begin{cases} \dfrac{\pi}{2}\alpha_i, & 0 \le t \le T_b \\ \dfrac{\pi}{2}(\alpha_i + \alpha_{i+1}), & T_b \le t \le 2T_b \end{cases}$$

Given the 16 possible combinations of output pair $(\alpha_i, \alpha_{i+1})$ and initial phase $\phi_0$ as shown in Fig. 1, there are only two possible waveforms that can result for $s_I(t)$ and only four possible waveforms that can result for $s_Q(t)$. Figure 2 illustrates the two possible waveforms for $s_I(t)$, denoted by $s_i(t)$, $i = 0, 1$, and Fig. 3 illustrates the four possible waveforms for $s_Q(t)$, denoted by $s'_j(t)$, $j = 0, 1, 2, 3$. For each phase state transition in Fig. 1, the corresponding waveform pair $\big(s_i(t), s'_j(t)\big)$ is indicated on the associated branch. Note that the only difference between the expanded time-invariant trellis representation of OQPSK in Fig. 1 and the expanded time-invariant trellis of MIL-STD SOQPSK in Fig. 4 of [7] is the waveform pair $\big(s_i(t), s'_j(t)\big)$ on each transition branch. This is because the phase pulse for OQPSK is a step function, while the phase pulse for MIL-STD SOQPSK varies linearly with time over each bit interval [2,3,7].

### C. An Equivalent Transmitter Implementation of OQPSK

Analogous to MIL-STD SOQPSK, given the symbol interval trellis representation of OQPSK in Fig. 1 and the labeling of its I and Q waveforms in Figs. 2 and 3, we can express the indices of the specific

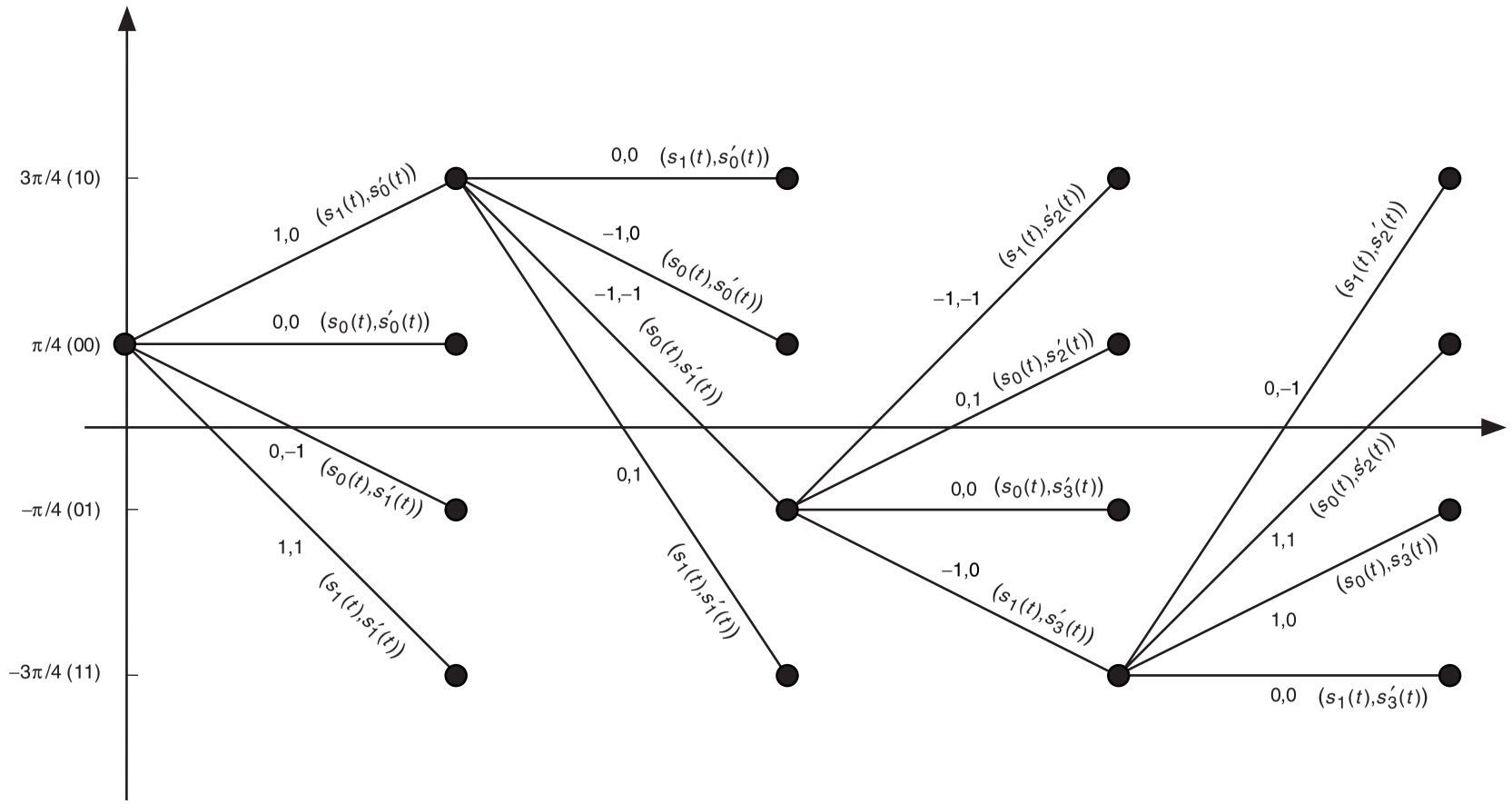


**Fig. 1. Expanded (branch leaving each state) time-invariant phase trellis of OQPSK.**

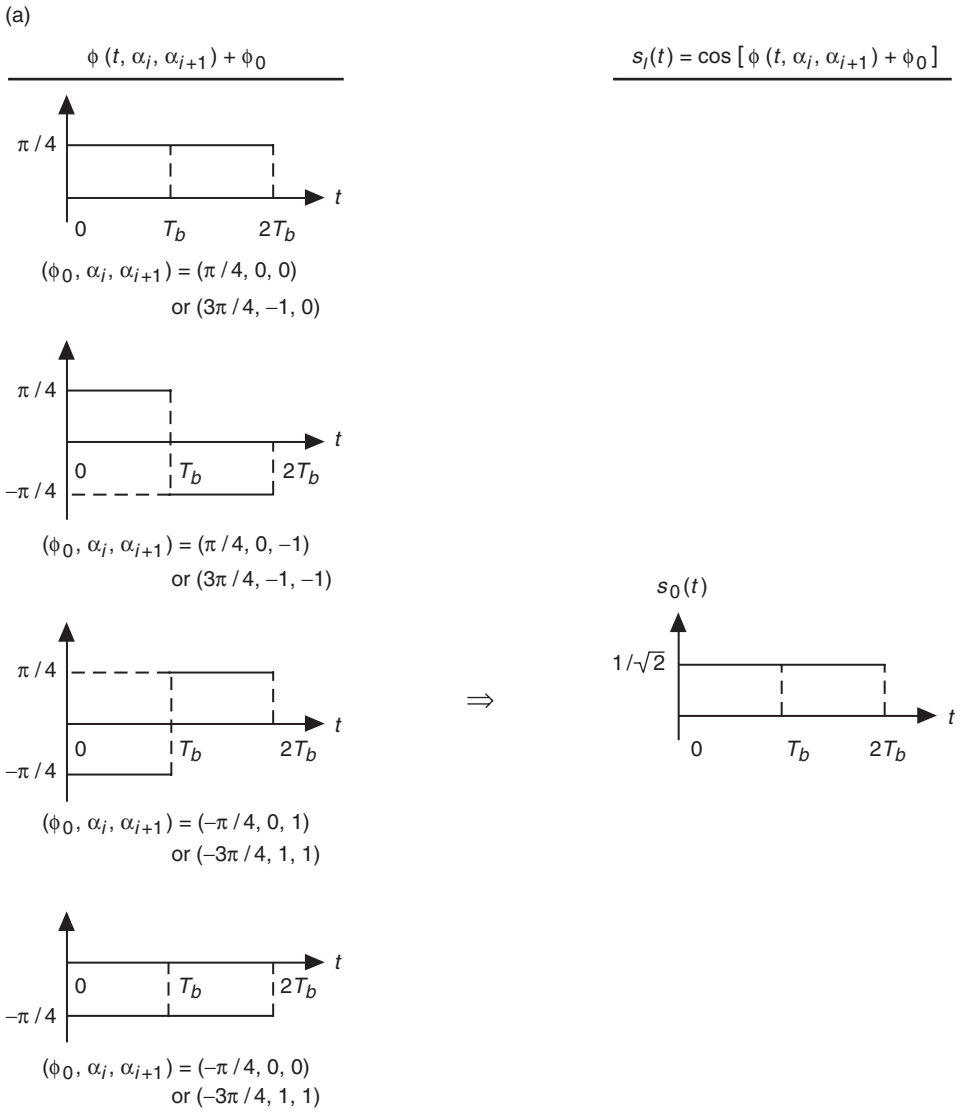


**Fig. 2. Two-bit phase sequences and corresponding in-phase (I) waveforms of OQPSK: (a) $s_0(t)$ and (b) $s_1(t)$.**

waveforms transmitted for $s_I(t)$ and $s_Q(t)$ in each symbol (2-bit) interval in terms of the two $\alpha$ values in this interval and the phase state at the beginning of the interval (which itself depends on the previous values of $\alpha$). Specifically, corresponding to $\alpha_i$ and $\alpha_{i+1}$ in the symbol interval $iT_b \le t \le (i+2)T_b$ ($i$ even) and phase state $\phi_i$ at the start of this interval, we have $s_I(t) = s_m(t)$ and $s_Q = s'_n(t)$, where the binary-coded decimal (BCD) representations of $m$ and $n$ are

$$m = \begin{cases} |\alpha_i|, & \text{if } \phi_i = \pm\pi/4 \\ 1 \oplus |\alpha_i|, & \text{if } \phi_i = \pm 3\pi/4 \end{cases}$$

$$n = \begin{cases} |\alpha_{i+1}|, & \text{if } \phi_i = \pi/4, 3\pi/4 \\ 2 + (1 \oplus |\alpha_{i+1}|), & \text{if } \phi_i = -\pi/4, -3\pi/4 \end{cases}$$

with "$\oplus$" denoting the "XOR" operation for binary $(0, 1)$ data. The BCD representations of $m$ and $n$ can be easily verified from Fig. 1.

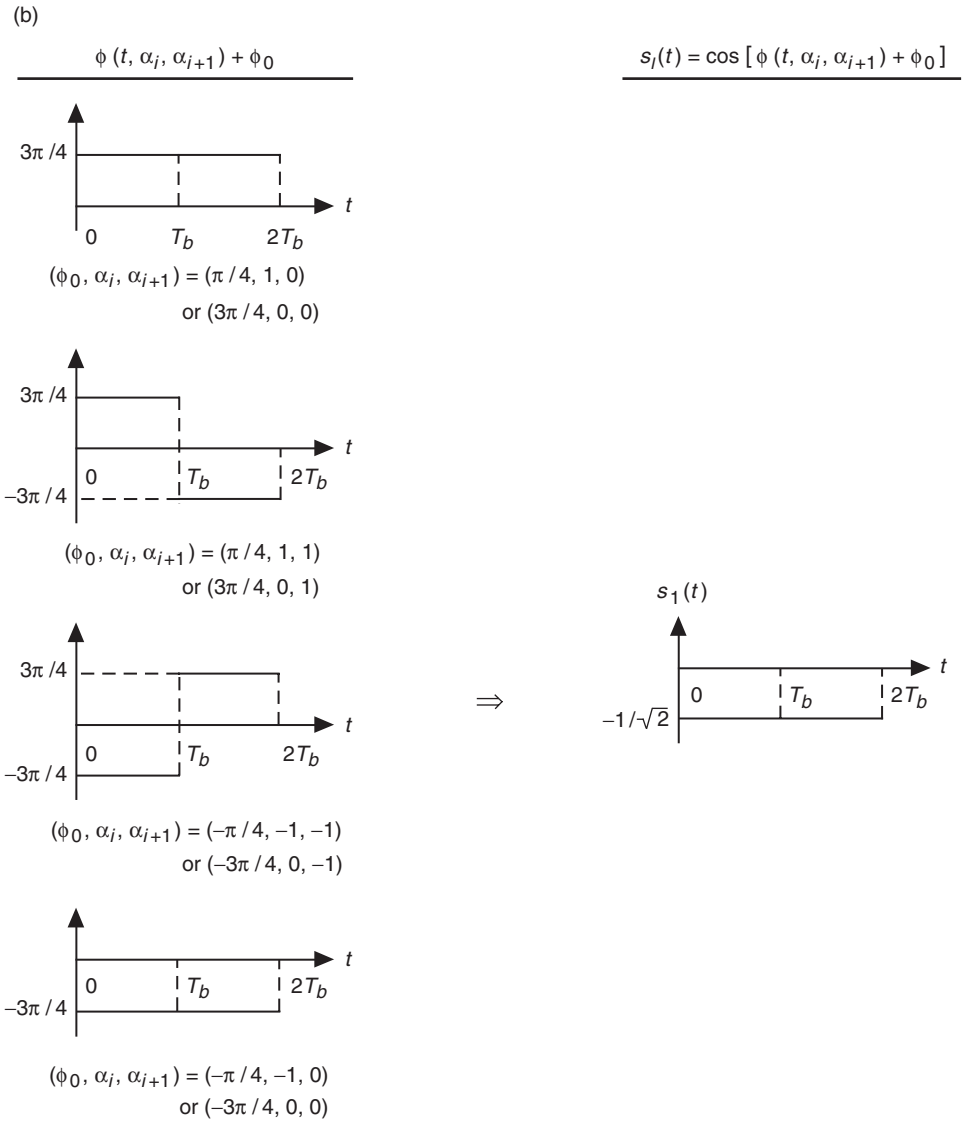


**Fig. 2 (cont'd.).**

A block diagram of the equivalent transmitter for OQPSK similar to that of MIL-STD SOQPSK in [7] is presented in Fig. 4 based on the above considerations. In this figure, the precoder operation is given by Eq. (1). Although each element of the precoder output is related to both the I and Q input bits according to Eq. (1), unlike MIL-STD SOQPSK, the signal mapping for OQPKS is not cross-correlated. That is, the I-channel waveform $s_I(t)$ is independent of the Q-channel input bits, and similarly, the Q-channel waveform $s_Q(t)$ is independent of the I-channel input bits. This will become apparent from the discussions in the next section.

## III. Interpretation of OQPSK and MIL-STD SOQPSK as Trellis-Coded Modulation

In the previous section, we expressed for OQPSK the indices of the specific waveforms transmitted for $s_I(t)$ and $s_Q(t)$ in terms of the two $\alpha$ values in each symbol interval and the starting phase at the beginning of each interval. We accomplished the same thing for MIL-STD SOQPSK in [7]. In this section, we will show for both OQPSK and MIL-STD SOQPSK that the indices of the transmitted waveforms for $s_I(t)$ and $s_Q(t)$ can be directly expressed in terms of the I- and Q-channel input binary $(0, 1)$ data.

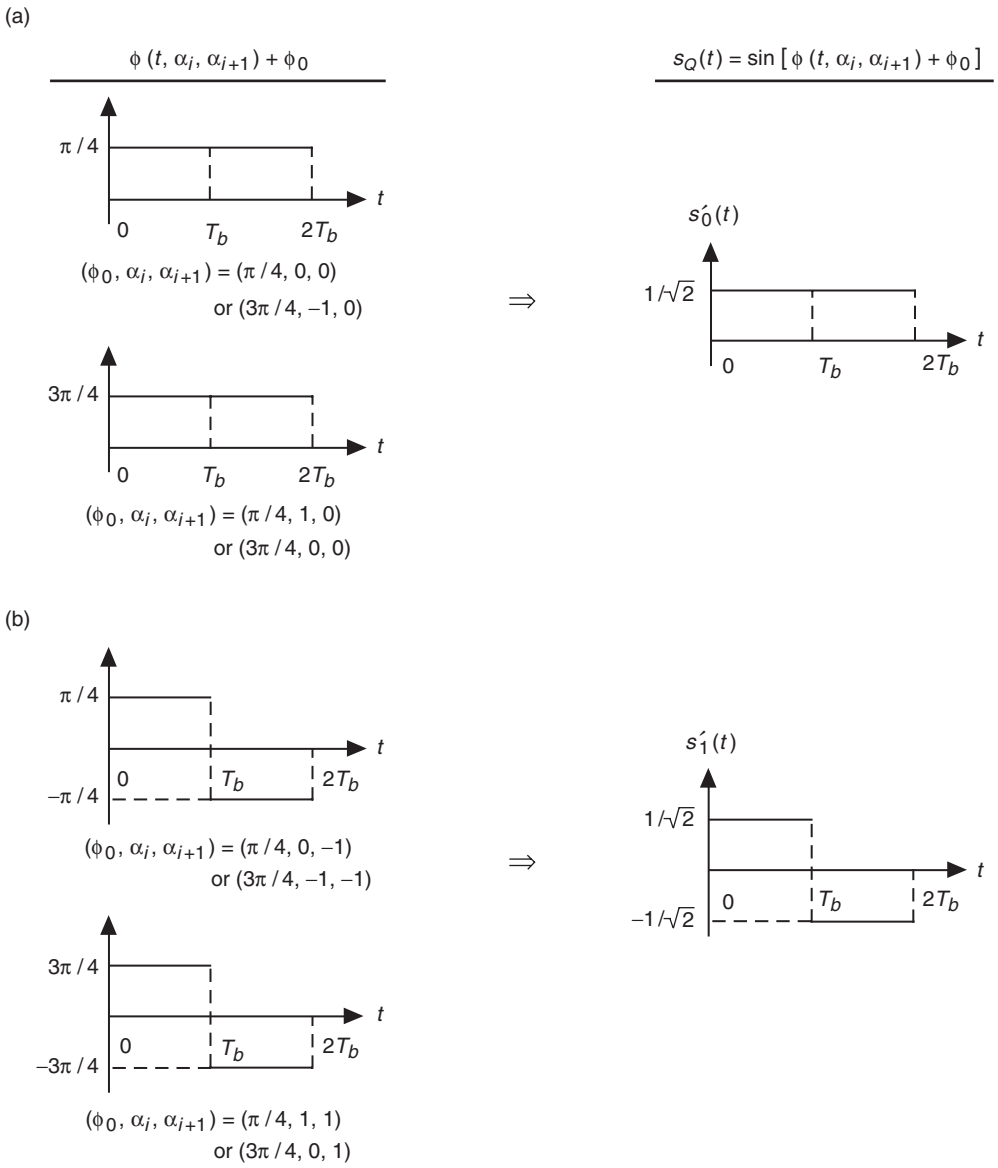


**Fig. 3. Two-bit phase sequences and corresponding quadrature-phase (Q) waveforms of OQPSK: (a) $s_0'(t)$, (b) $s_1'(t)$, (c) $s_2'(t)$, and (b) $s_3'(t)$.**

Specifically, in each symbol interval $n$, we denote the I and Q input binary data as $D_{I,n}$ and $D_{Q,n}$, respectively. Note that the phase state in the $(n-1)$th symbol interval is simply "$D_{I,n-1}D_{Q,n-1}$," and it will become "$D_{I,n}D_{Q,n}$" in the $n$th symbol interval with the input data $D_{I,n}$ and $D_{Q,n}$. Therefore, given the indices of the corresponding output waveform pair $\big(s_I(t), s_Q(t)\big)$ as indicated on each branch in the trellis representations of OQPSK and MIL-STD SOQPSK, it is straightforward to express the indices in terms of the input data. In particular, assume that the output waveform pair is $\big(s_i(t), s_j'(t)\big)$ in the $n$th symbol interval, and define the indices $i$ and $j$ by

$$i = I_2 \times 2^2 + I_1 \times 2^1 + I_0 \times 2^0$$

$$j = Q_2 \times 2^2 + Q_1 \times 2^1 + Q_0 \times 2^0$$

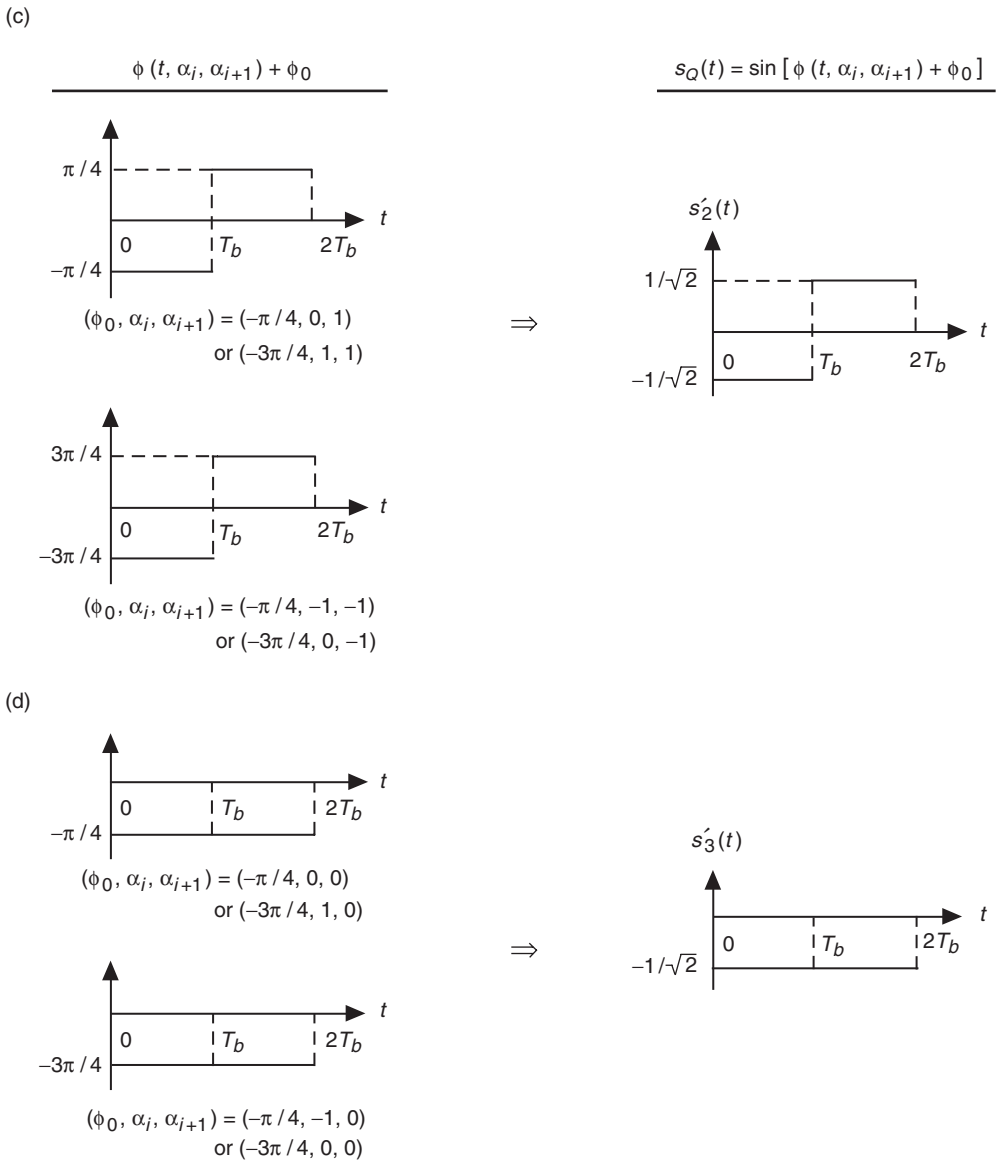


**Fig. 3 (cont'd.).**

then for MIL-STD SOQPSK,

$$\begin{cases} I_2 = D_{I,n-1} & Q_2 = D_{Q,n-1} \\ I_1 = D_{I,n} \oplus D_{I,n-1} & Q_1 = D_{I,n} \oplus D_{I,n-1} = I_1 \\ I_0 = D_{Q,n} \oplus D_{Q,n-1} & Q_0 = D_{Q,n} \oplus D_{Q,n-1} = I_0 \end{cases}$$

and for OQPSK,

$$\begin{cases} I_2 = 0 & Q_2 = 0 \\ I_1 = 0 & Q_1 = D_{Q,n-1} \\ I_0 = D_{I,n} & Q_0 = D_{Q,n} \end{cases}$$

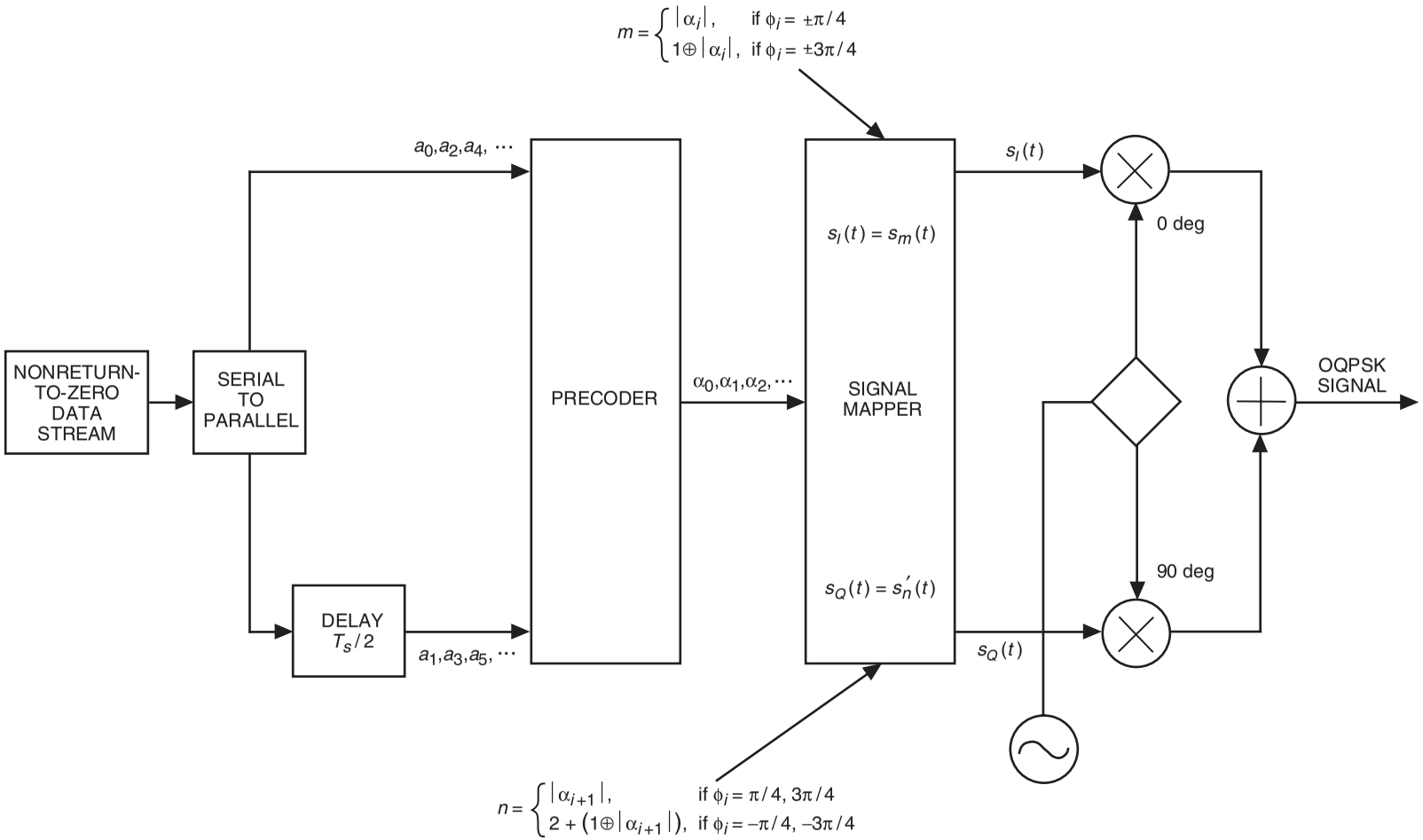


**Fig. 4. Equivalent transmitter for OQPSK.**

Graphical illustration of the implementations of MIL-STD SOQPSK and OQPSK based on the above mappings is given in Fig. 5. For MIL-STD SOQPSK, the eight waveforms $s_i(t), i = 0, \cdots, 7$ are given in Fig. 5 of [7], and the eight waveforms $s'_j(t), j = 0, \cdots, 7$ are given in Fig. 6 of [7]. For OQPSK, the two waveforms $s_i(t), i = 0, 1$, are illustrated in Fig. 2, and the four waveforms $s'_j(t), j = 0, \cdots, 3$ are illustrated in Fig. 3. From Fig. 5(a) we see that MIL-STD SOQPSK can be clearly decomposed into a 4-state trellis encoder and a memoryless signal mapper. This inherent 4-state trellis encoder of MIL-STD SOQPSK has two binary $(0, 1)$ inputs $D_{I,n}$ and $D_{Q,n}$, and two waveform outputs $s_i(t), s'_j(t)$, where the trellis state is defined by the 2-bit sequence $D_{I,n-1}$ and $D_{Q,n-1}$. The trellis of this 4-state encoder is exactly the one illustrated by Fig. 4 in [7]. Since both the I- and Q-channel output waveform indices depend on the cross-channel input data in addition to their own channel input data, it is obvious that MIL-STD SOQPSK is a form of XTCQM. Similarly, from Fig. 5(b) we see that OQPSK can be interpreted as being composed of a "degraded" 4-state trellis encoder and a memoryless signal mapper.[3] The trellis of this degraded trellis encoder is exactly the one depicted in Fig. 1. For OQPSK, it is obvious from Fig. 5(b) that the I- and Q-channel output waveform indices depend only on their own channel input data. Therefore, independent I- and Q-channel detection is possible for OQPSK.

Note that the decomposition of OQPSK and MIL-STD SOQPSK into a (degraded) trellis encoder and a memoryless mapper is important since, as will be shown in Section VI, it allows iterative decoding of the outer codes and these inherent trellis codes in their corresponding coded systems.

## IV. Receiver Structures for MIL-STD SOQPSK

In accordance with the foregoing representation of MIL-STD SOQPSK as a trellis-coded modulation with four states, in this section we present the corresponding optimum receiver structure and propose a simplified receiver structure for it.

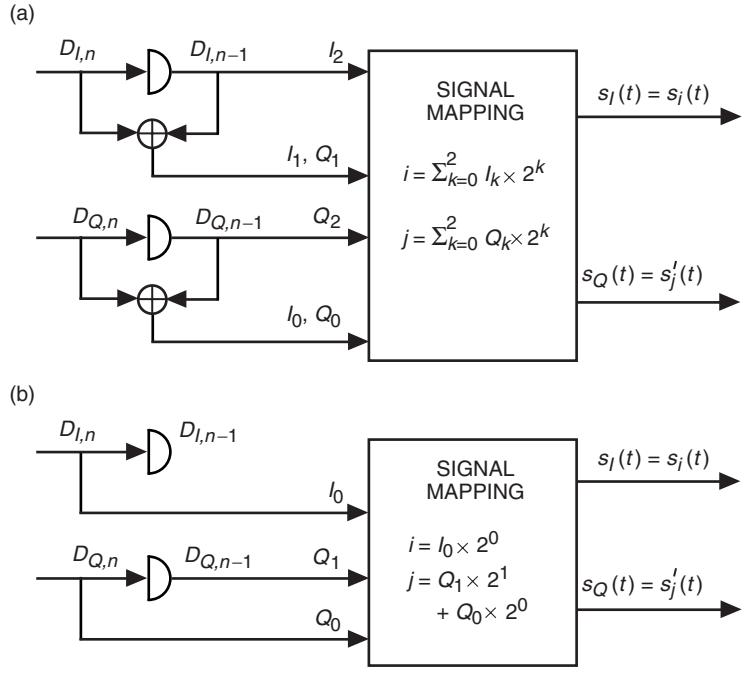


**Fig. 5. Alternative implementations of MIL-STD SOQPSK and OQPSK baseband signals: (a) MIL-STD SOQPSK and (b) OQPSK.**

[3] By "degraded" trellis encoder we mean a degenerate form of such an encoder having no memory.

### A. Optimum Receiver

The optimum receiver employing a Viterbi algorithm (VA) is illustrated in Fig. 6. It consists of a bank of 8 matched filters (4 in each of the I and Q channels) followed by a 4-state trellis decoder. Note that although members of the I and Q signaling sets $s_i(t)$ and $s'_j(t)$ $(i, j = 0, 1, \cdots, 7)$ do not all have equal energy, it can be shown that because the sum of the energies from allowable pairs of I and Q signals is constant, energy biases in the matched filters are not necessary when the matched-filter outputs are used in a Viterbi algorithm. Specifically, let us first analytically characterize the two sets of 8 baseband waveforms $s_i(t), s'_j(t)$ $(i, j = 0, 1, \cdots, 7)$ illustrated in Figs. 5 and 6 of [7] that represent all possible transmitted signals for $s_I(t)$ and $s_Q(t)$, respectively. Assuming that the bit duration is $T_b$ and the symbol duration $T_s = 2T_b$, we have

$$s_0(t) = \frac{1}{\sqrt{2}}, \quad 0 \le t \le 2T_b$$

$$s_1(t) = \begin{cases} \dfrac{1}{\sqrt{2}}, & 0 \le t \le T_b \\ \cos\left[\dfrac{\pi}{2T_b}(t - T_b) - \dfrac{\pi}{4}\right], & T_b \le t \le 2T_b \end{cases}$$

$$s_2(t) = \begin{cases} \cos\left(\dfrac{\pi}{2T_b} + \dfrac{\pi}{4}\right), & 0 \le t \le T_b \\ -\dfrac{1}{\sqrt{2}}, & T_b \le t \le 2T_b \end{cases}$$

$$s_3(t) = \cos\left(\frac{\pi}{2T_b} + \frac{\pi}{4}\right), \quad 0 \le t \le 2T_b$$

$$s'_0(t) = \frac{1}{\sqrt{2}}, \quad 0 \le t \le 2T_b$$

$$s'_1(t) = \begin{cases} \dfrac{1}{\sqrt{2}}, & 0 \le t \le T_b \\ \cos\left[\dfrac{\pi}{2T_b}(t - T_b) + \dfrac{\pi}{4}\right], & T_b \le t \le 2T_b \end{cases}$$

$$s'_2(t) = \begin{cases} \cos\left(\dfrac{\pi}{2T_b} - \dfrac{\pi}{4}\right), & 0 \le t \le T_b \\ \dfrac{1}{\sqrt{2}}, & T_b \le t \le 2T_b \end{cases}$$

$$s'_3(t) = \cos\left(\frac{\pi}{2T_b} - \frac{\pi}{4}\right), \quad 0 \le t \le 2T_b$$

and in addition,

$$s_{4+i}(t) = -s_i(t), \quad i = 0, 1, 2, 3$$

$$s'_{4+j}(t) = -s'_j(t), \quad j = 0, 1, 2, 3$$

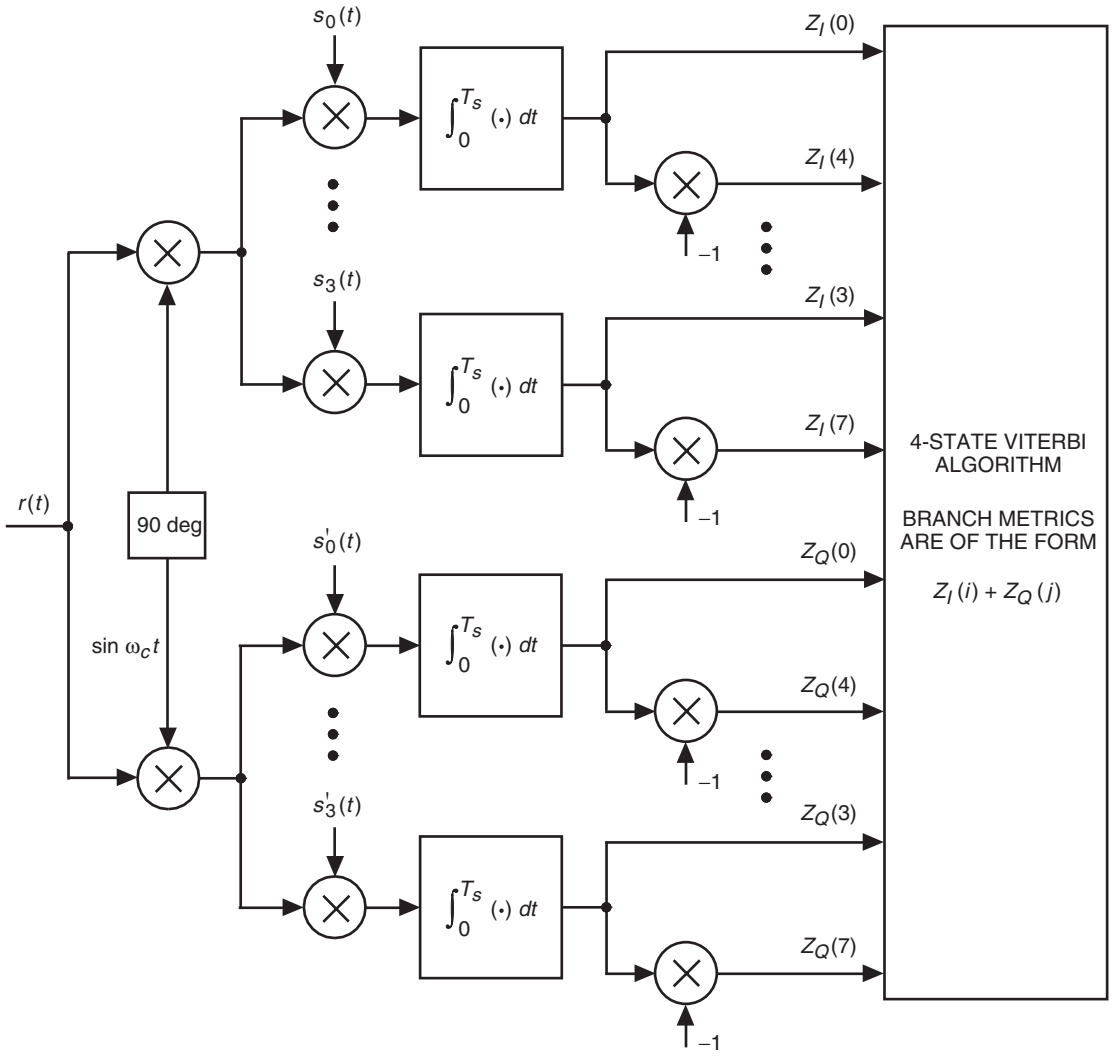


**Fig. 6. Optimum receiver structure for MIL-STD SOQPSK.**

Then it is easily shown from the expressions of $s_i(t)$ and $s'_j(t)$ $(i, j = 0, 1, \cdots, 7)$ that the energy per symbol for each waveform is

$$E_0 = E_4 = E'_0 = E'_4 = \frac{T_s}{2}$$

$$E_1 = E_5 = E'_2 = E'_6 = \left(\frac{1}{2} + \frac{1}{2\pi}\right) T_s$$

$$E_2 = E_6 = E'_1 = E'_5 = \left(\frac{1}{2} - \frac{1}{2\pi}\right) T_s$$

$$E_3 = E_7 = E'_3 = E'_7 = \frac{T_s}{2}$$

with $E_i, E'_j$ $(i, j = 0, 1, \cdots, 7)$ denoting the energy for $s_i(t)$ and $s'_j(t)$, respectively. Therefore,

$$E_i + E_i' = E_i + E_{4+i}' = E_{4+i} + E_i' = E_{4+i} + E_{4+i}' = T_s, \quad i = 0, 1, 2, 3$$

Since from Fig. 4 of [7] we see that the possible output waveform pairs for $s_I(t)$ and $s_Q(t)$ of MIL-STD SOQPSK are of the form $\big(s_i(t), s_i'(t)\big)$, $\big(s_i(t), s_{4+i}'(t)\big)$, $\big(s_{4+i}(t), s_i'(t)\big)$, and $\big(s_{4+i}(t), s_{4+i}'(t)\big)$, $i = 0, 1, 2, 3$, all I and Q waveform pairs have the same total energy. Thus, it is not necessary to set the energy biases in the matched filters in Fig. 6.

### B. Simplified Receiver

In a desire to reduce the complexity of the optimum receiver in Fig. 6 with the hope of not sacrificing significant power efficiency, a simplified receiver can be formed by grouping sets of waveforms together based on their similarities. In particular, the 8 waveforms of the I-channel output $s_I(t)$ are divided into 4 groups, and so are the 8 waveforms of the Q-channel output $s_Q(t)$. For $s_I(t)$, the $i$th ($i = 0, 1, 2, 3$) group consists of waveforms $s_{2i}(t)$ and $s_{2i+1}(t)$. For $s_Q(t)$, when $i = 0, 2$, the $i$th group consists of waveforms $s_{2i}'(t)$ and $s_{2i+2}'(t)$, and, when $i = 1, 3$, of waveforms $s_{2i-1}'(t)$ and $s_{2i+1}'(t)$. By defining $q_i(t)$ and $q_i'(t)$ ($i = 0, 1, 2, 3$) as the average of the waveforms in each group for $s_I(t)$ and $s_Q(t)$, respectively, we have

$$q_i(t) = \frac{1}{2}\big[s_{2i}(t) + s_{2i+1}(t)\big], \quad i = 0, 1, 2, 3$$

$$q_i'(t) = \begin{cases} \dfrac{1}{2}\left[s_{2i}'(t) + s_{2i+2}'(t)\right], & i = 0, 2 \\ \dfrac{1}{2}\left[s_{2i-1}'(t) + s_{2i+1}'(t)\right], & i = 1, 3 \end{cases}$$

Note that since $s_{4+i}(t) = -s_i(t)$ and $s_{4+i}'(t) = -s_i'(t)$, $i = 0, 1, 2, 3$, we have

$$\begin{aligned} q_{2+i}(t) &= -q_i(t), \\ q_{2+i}'(t) &= -q_i'(t), \end{aligned} \qquad i = 0, 1$$

Figure 7 illustrates the waveforms for $q_i(t)$ and $q_i'(t)$ ($i = 0, 1$). The waveforms for $q_{2+i}(t)$ and $q_{2+i}'(t)$ ($i = 0, 1$) are of the same shape as those of $q_i(t)$ and $q_i'(t)$ but with opposite signs.

Now we replace the waveform assignments of the group members for $s_I(t)$ and $s_Q(t)$ by their corresponding average waveform, i.e., $s_0(t)$ and $s_1(t)$ both become $q_0(t)$; $s_2(t)$ and $s_3(t)$ both become $q_1(t)$, and so on. Then, because of the relation between the I and Q coded bits and the BCD signal mapping in Fig. 5(a), the cross-correlation between the I and Q channel would disappear. This is because what distinguishes the two waveforms in each group for $s_I(t)$ is the least-significant bit $I_0$, and it is the middle bit $Q_1$ for $s_Q(t)$. If no distinction needs to be made in each group, we can simply drop the bits $I_0$ and $Q_1$ and just use the remaining two bits, $I_2, I_1$ and $Q_2, Q_0$, in each channel to specify the transmitted waveform pair $\big(q_i(t), q_j'(t)\big)$, $i, j = 0, 1, 2, 3$. That is,

$$i = I_2 \times 2 + I_1$$

$$j = Q_2 \times 2 + Q_0$$

By inspecting Fig. 5(a), we see that this is equivalent to the I-channel signal being chosen based only on the I-encoder outputs and the Q-channel signal being chosen based only on the Q-encoder outputs.

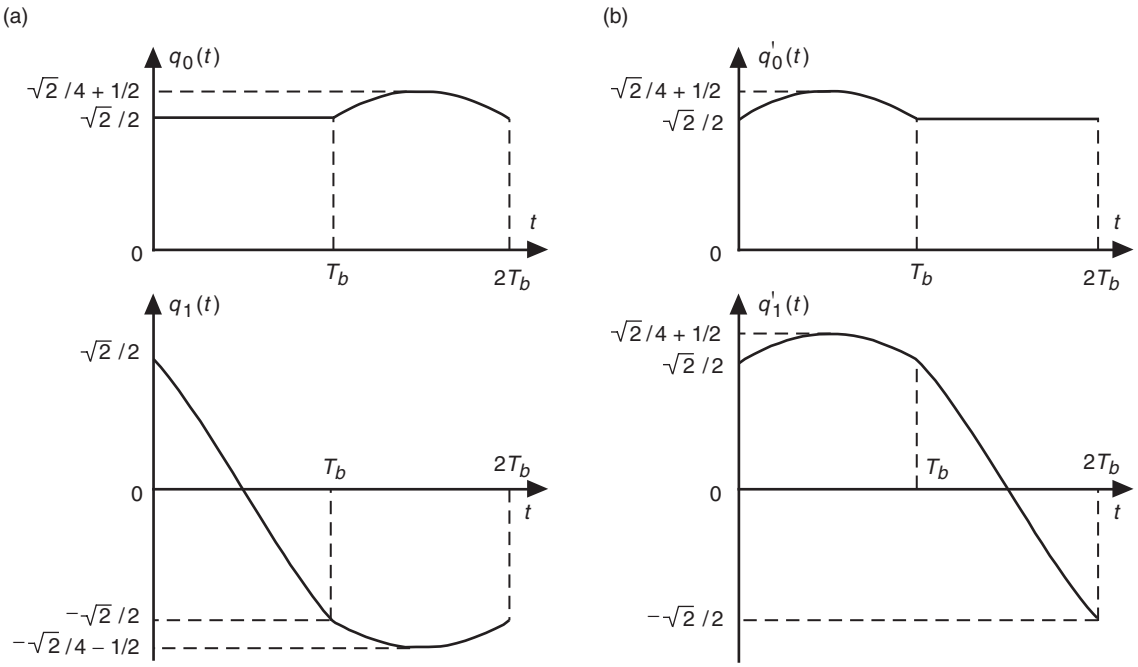


**Fig. 7. Simplified waveforms (a) $q_i(t)$ and (b) $q_i'(t)$ ($i = 0, 1$) for MIL-STD SOQPSK .**

Thus, the cross-correlation of the encoder outputs in choosing the I and Q waveforms disappears, and the trellis structure of the modulation decouples into two independent (I and Q) 2-state trellises.

The simplified Viterbi receiver corresponding to the 2-state trellises is illustrated in Fig. 8. In this simplified receiver, the I and Q decisions are separately generated by individual 2-state VAs using the energy-biased correlations derived from the I and Q demodulated signals, respectively. Note that since the energy per symbol is different for $q_i(t)$ and $q_{i+1}(t)$ $(i = 0, 2)$ as well as for $q_i'(t)$ and $q_{i+1}'(t)$ $(i = 0, 2)$, the energy biases must be set in the matched-filter outputs as shown in Fig. 8. In this figure, $\bar{E}_i$ and $\bar{E}_i'$ denote the energy per symbol for $q_i(t)$ and $q_i'(t)$ $(i = 0, 1)$, respectively. It is obvious from Fig. 7 that $\bar{E}_i = \bar{E}_i'$, $i = 0, 1, 2, 3$. In addition, it is easily calculated that $\bar{E}_0 = \bar{E}_0' = (1/2) + (1/4\pi)$, and that $\bar{E}_1 = \bar{E}_1' = (1/2) - (1/4\pi)$. Of course, the two VAs for the I and Q channels can be combined into a single 4-state VA if desired. Compared to the optimum Viterbi receiver, the simplified one reduces the number of correlators by half. This simplified receiver for MIL-STD SOQPSK is very similar to the one for FQPSK described in [17] in both structure and complexity.

## V. Performance Comparison of Uncoded OQPSK, MIL-STD SOQPSK, and FQPSK

In this section, we first analyze the asymptotic BER Performance of MIL-STD SOQPSK using two different methods and then compare the simulated BER performance of uncoded MIL-STD SOQPSK with both the optimum receiver and the simplified receiver to that of OQPSK and FQPSK.

### A. Asymptotic BER Performance of MIL-STD SOQPSK

In this subsection, we obtain an expression for the minimum Euclidean distance associated with the symbol-by-symbol trellis representation of MIL-STD SOQPSK shown in Fig. 4 of [7].

Supposing that the initial phase state is $(\pi/4)(00)$ and the all-zero sequence is transmitted, from Fig. 4 of [7] we see that there is a path of length 2 that starts and ends at the same phase state $(\pi/4)(00)$ but differs from the all-zero sequence path. This shortest-length path is illustrated in Fig. 9 with the

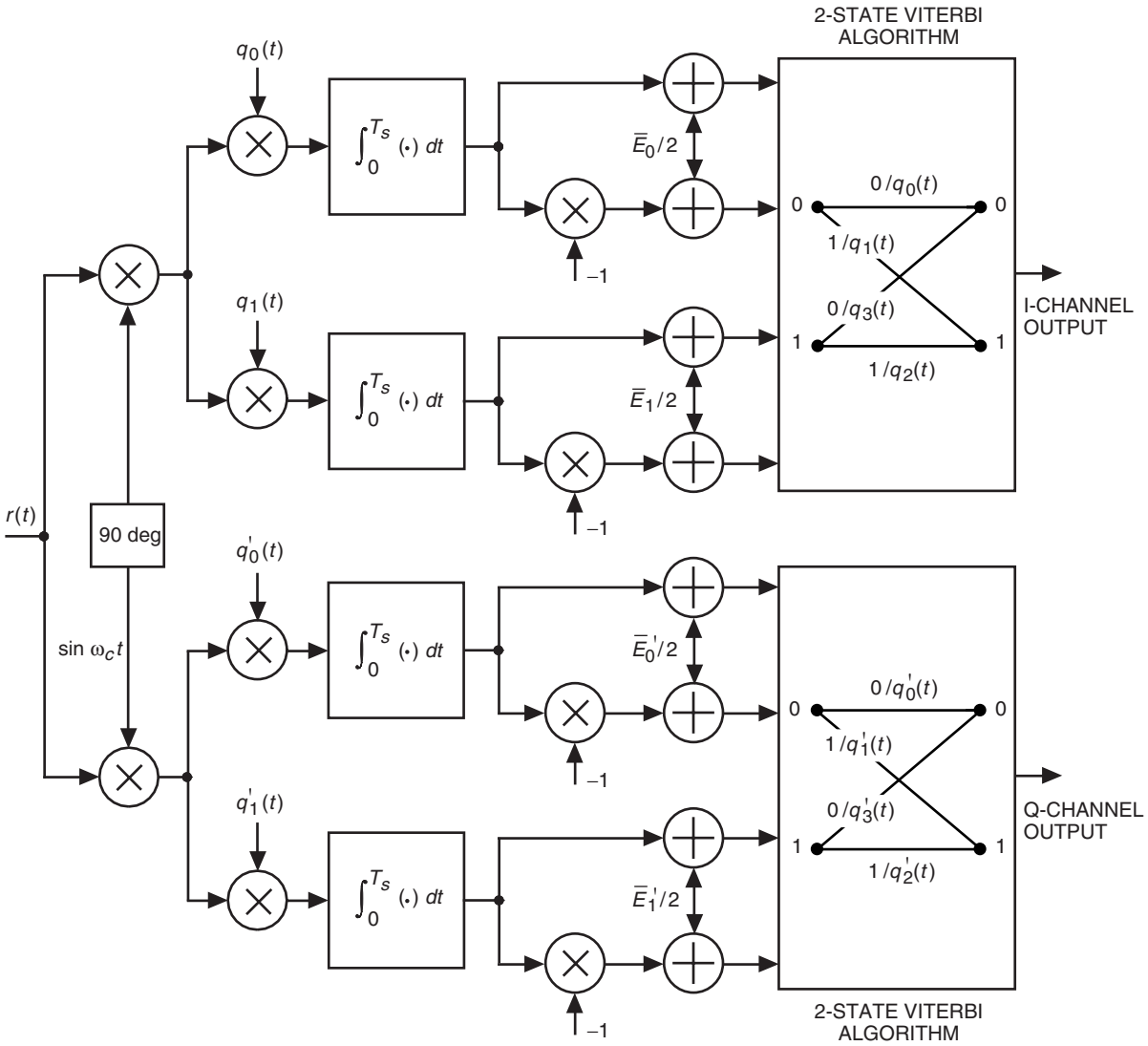


**Fig. 8. The simplified Viterbi receiver for MIL-STD SOQPSK.**

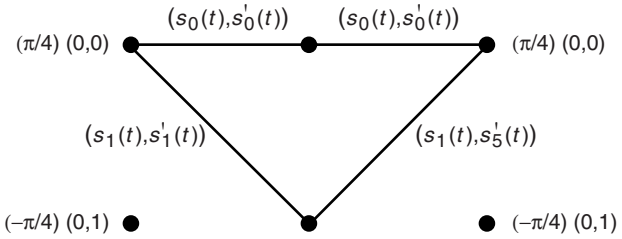


**Fig. 9. Shortest-length error-event path of MIL-STD SOQPSK.**

output waveforms for $s_I(t)$ and $s_Q(t)$ indicated on each branch. The corresponding minimum squared Euclidean distance is

$$\begin{aligned} d^2_{\min} &= \int_0^{T_s} \left[2|s_1(t) - s_0(t)|^2 + |s'_1(t) - s'_0(t)|^2 + |s'_5(t) - s'_0(t)|^2\right] dt \\ &= 2\int_0^{T_b} \left[\cos\left(\frac{\pi}{2T_b} - \frac{\pi}{4}\right) - \frac{1}{\sqrt{2}}\right]^2 dt \\ &\quad + \int_0^{T_b} \left[\cos\left(\frac{\pi}{2T_b} + \frac{\pi}{4}\right) - \frac{1}{\sqrt{2}}\right]^2 dt \\ &\quad + \int_0^{T_b} \left[-\cos\left(\frac{\pi}{2T_b} + \frac{\pi}{4}\right) - \frac{1}{\sqrt{2}}\right]^2 dt \\ &\quad + \int_0^{T_b} \left(-\frac{1}{\sqrt{2}} - \frac{1}{\sqrt{2}}\right)^2 dt \\ &= \left(3 - \frac{4}{\pi}\right) T_s \end{aligned}$$

The average signal (I + Q) energy per symbol $E_{av}$ is obtained from

$$\begin{aligned} E_{av} = 2E_b &= \frac{1}{8}\sum_{i=0}^{7} \int_0^{2T_b} |s_i(t)|^2 + |s'_i(t)|^2 dt \\ &= T_s \end{aligned}$$

where $E_b$ is the average energy per bit. Therefore, the normalized minimum squared Euclidean distance is

$$\frac{d^2_{\min}}{2E_b} = 3 - \frac{4}{\pi} \doteq 1.727 \tag{2}$$

Examination of other length-2 error event paths relative to transmitted sequences other than the all-zero sequence reveals that the smallest value of normalized squared Euclidean distance is still given by Eq. (2). Furthermore, error event paths longer than length-2 correspond to larger values of squared Euclidean distance. Thus, the normalized minimum squared Euclidean distance for MIL-STD SOQPSK is given by Eq. (2).

An alternative method for obtaining the result in Eq. (2) is by using the bit-by-bit CPM representation of MIL-STD SOQPSK. In particular, suppose two MIL-STD SOQPSK signals $s(t)$ and $s'(t)$ differ over $N$ bit intervals, i.e., their corresponding effective data sequences $\boldsymbol{\alpha}$ and $\boldsymbol{\alpha}'$ differ over $N$ $T_b$-intervals. Let $\boldsymbol{\gamma}$ be the length-$N$ difference sequence between $\boldsymbol{\alpha}$ and $\boldsymbol{\alpha}'$, i.e., $\boldsymbol{\gamma}$ is an $N$-bit subsequence of $\boldsymbol{\alpha} - \boldsymbol{\alpha}'$ that starts and ends with a non-zero element. Then, it is shown in [19] that the Euclidean distance between the two CPM signals can be expressed as

$$d^2\big(s(t), s'(t)\big) = \frac{2E_b}{T_b}\int_0^{NT_b}\big[1-\cos\phi(t,\boldsymbol{\gamma})\big]dt$$

To obtain the minimum Euclidean distance, one must find the corresponding difference sequence $\boldsymbol{\gamma}_{\min}$. Computer simulation search in [5] shows that, for SOQPSK, $\boldsymbol{\gamma}_{\min} = (1, 0, -1)$. Therefore, according to the MIL-STD SOQPSK phase modulation process [7],

$$\phi(t,\boldsymbol{\gamma}_{\min}) = \begin{cases} \dfrac{\pi t}{2T_b}, & 0 \le t \le T_b \\ \dfrac{\pi}{2}, & T_b \le t \le 2T_b \\ \dfrac{\pi}{2} - \dfrac{\pi t}{2T_b}, & 2T_b \le t \le 3T_b \end{cases}$$

and the minimum squared Euclidean distance is easily calculated as

$$d^2_{\min} = \frac{2E_b}{T_b}\int_0^{3T_b}\big[1-\cos\phi(t,\boldsymbol{\gamma}_{\min})\big]dt$$

$$= \left(3 - \frac{4}{\pi}\right)\cdot 2E_b$$

Thus, $(d^2_{\min}/2E_b) = 3 - (4/\pi) \doteq 1.727$, which is the same as in Eq. (2). When compared to OQPSK, which has the same normalized minimum squared Euclidean distance as BPSK, i.e., $(d^2_{\min}/2E_b) = 2.0$, there is a loss of 0.638 dB for MIL-STD SOQPSK. In addition, when compared to FQPSK, which is more spectrally efficient (see Figs. 6 and 9 in [3]) and for which it was shown in [9,10] that $(d^2_{\min})/(2E_b) = 1.56$, there is an asymptotic gain of 0.441 dB for MIL-STD SOQPSK.

### B. Simulation Results

We have simulated the optimum receiver structure shown in Fig. 6 for uncoded MIL-STD SOQPSK as well as the simplified receiver structure shown in Fig. 8. The numerical results are illustrated in Fig. 10. Also shown in Fig. 10 are the simulated BER performance of FQPSK with the optimum receiver and with a simplified receiver, which are taken from [9,10,17]. Furthermore, in Fig. 10 we also have given the simulated BER performance of uncoded OQPSK, which provides a lower bound for both MIL-STD SOQPSK and FQPSK. To simulate the performance of OQPSK with Viterbi decoding, the bit-interval 8-state trellis illustrated in Fig. 2 of [7] is used. In addition, we also have simulated the case where the symbol-interval trellis representation of OQPSK illustrated in Fig. 1 is used. The simulation results using these two different trellis representations of OQPSK with a Viterbi decoder turn out to be the same, and they also match the theoretical BER of BPSK and QPSK, which coincides with the conclusion of Lee.[4]

From Fig. 10 we see that, at BER $= 10^{-5}$, MIL-STD SOQPSK with the optimum receiver is about 0.308 dB worse than OQPSK, but is about 0.46 dB better than FQPSK with optimal receiving. The simplified MIL-STD SOQPSK receiver has a performance that is very close to the optimum receiver: at BER $= 10^{-5}$, the $E_b/N_0$ loss is only about 0.115 dB. For FQPSK, the performance gap between the simplified receiver and the optimum one is bigger: the $E_b/N_0$ loss at BER $= 10^{-5}$ is roughly 0.27 dB. The smaller performance gap between the simplified receiver and the optimum receiver for MIL-STD SOQPSK

[4] D. Lee, "OQPSK with CPM Demodulation Using Viterbi Algorithm," JPL Interoffice Memorandum (internal document), Jet Propulsion Laboratory, Pasadena, California, May 2003.

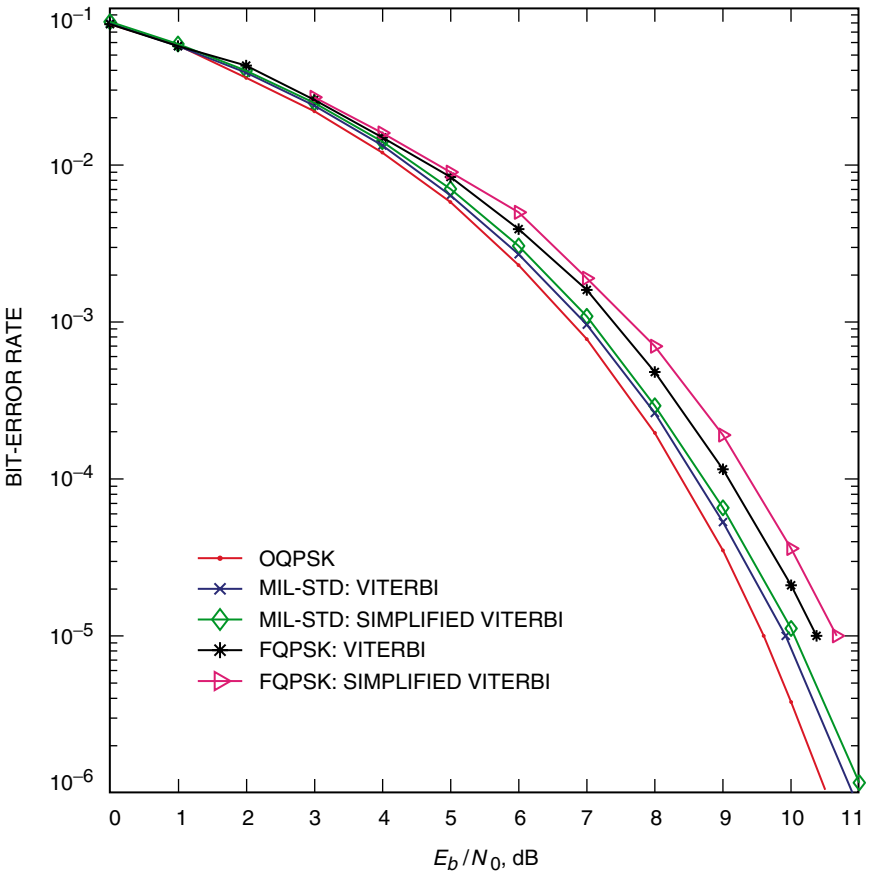


**Fig. 10. BER performance comparison of uncoded systems.**

is due to the fact that the simplified MIL-STD SOQPSK receiver reduces the number of matched filters in the optimum receiver by only a factor of one-half, while the simplified FQPSK receiver reduces it by a factor of three-quarters.

## VI. Coded OQPSK and MIL-STD SOQPSK with Iterative Decoding

Since both OQPSK and MIL-STD SOQPSK have inherent trellis codes as shown in Fig. 5, these trellis codes can be viewed as the inner code of a concatenated code in coded OQPSK and MIL-STD SOQPSK systems. As was true for the FQPSK applications [11–13], in order to realize coding gains from the concatenation of the outer code and the inherent inner code of OQPSK or MIL-STD SOQPSK, the I and Q inner encoders of the equivalent transmitters in Fig. 5 must be replaced by their recursive equivalents. Therefore, before presenting the serial and parallel concatenated coding structures for coded OQPSK and MIL-STD SOQPSK systems and introducing the simplified iterative decoding process for MIL-STD SOQPSK, we first describe the recursive I and Q encoders for both OQPSK and MIL-STD SOQPSK.

### A. Recursive I and Q Encoders of OQPSK and MIL-STD SOQPSK

For OQPSK and MIL-STD SOQPSK, given the original trellis of each non-recursive I or Q encoder, the remapped recursive encoder must have a trellis for which the output bits corresponding to each transition between states remain unchanged. The only changes allowed are the input bit(s) associated with each transition. This is to guarantee that the allowable OQPSK or MIL-STD SOQPSK encoder output sequences remain unchanged so that the remapping does not change the envelope and spectral characteristics of the modulated signals. Under this consideration, it easily can be shown that only one

recursive version is allowed for each of the encoders in Fig. 5, and the recursive equivalents of these encoders are illustrated in Fig. 11. It is obvious from Fig. 5 that the I and Q encoders are the same for MIL-STD SOQPSK, and so are their recursive equivalents, shown in Fig. 11. For OQPSK, the I and Q encoders are also the same if we view the I channel as having a degraded encoder, with only one output bit instead of two. Therefore, their recursive equivalents are also the same except that the I encoder has only one output bit. The trellis diagrams of the original as well as the remapped encoders for OQPSK and MIL-STD SOQPSK are shown in Figs. 12 and 13, respectively.

Note that if we replace the original encoders of OQPSK and MIL-STD SOQPSK shown in Fig. 5 with their recursive equivalents shown in Fig. 11, simulation results (not illustrated) show that the BERs of the uncoded OQPSK and MIL-STD SOQPSK are now twice those of the original systems shown in Fig. 10. However, for the coded cases, the recursive versions of the encoders provide significant coding gains, which will be demonstrated through a few examples in the following subsections.

### B. Serial Concatenation

We first consider the serial concatenated coded OQPSK and MIL-STD SOQPSK systems illustrated in Fig. 14. Here the input data first are encoded by an outer encoder, interleaved, and then applied to the I and Q channels of the equivalent baseband transmitter for OQPSK or the equivalent baseband transmitter for MIL-STD SOQPSK shown in Fig. 5, where the I and Q inner encoders are replaced by their recursive counterparts in Fig. 11. After transmission over the additive white Gaussian noise (AWGN) channel, for MIL-STD SOQPSK, the received signals of the I and Q channels are passed through a bank of 8 matched filters to generate a total of 16 correlator outputs, as shown in Fig. 6. For OQPSK, the I-channel received signal is passed through one matched filter, and the Q-channel received signal is passed through two matched filters to generate a total of 6 correlator outputs. These correlator outputs then are used by a 4-state soft-input soft-output (SISO) iterative decoder as branch metrics. For OQPSK, since there is no correlation between the I channel and the Q channel, two separate 2-state iterative decoders can be used instead of a combined 4-state decoder. These two decoding schemes have the same BER performance, which is verified by our simulations. For MIL-STD SOQPSK, the 4-state joint I- and Q-channel iterative decoder must be used since there exist correlations between these two channels. Note that in addition to the SISO module for decoding the inner code provided by OQPSK or MIL-STD SOQPSK, there is also a SISO module for decoding the outer code.

Based on the correlator outputs, the inner SISO decoder(s) provides extrinsic information (additional reliabilities) associated with the OQPSK or MIL-STD SOQPSK encoder input bits to the outer SISO decoder. The outer decoder in turn provides enhanced versions of these extrinsics (reliabilities) using the outer code structure. These enhanced reliabilities of the OQPSK or MIL-STD SOQPSK encoder input bits are fed back to the inner SISO decoder(s) after appropriate interleaving. With these feedback reliabilities as well as the correlator outputs, the inner SISO decoder(s) will be able to provide updated extrinsic information to the outer SISO decoder about the outer encoder outputs. This process iterates a given number of times and, at the end of the last iteration, the outer SISO decoder produces a decision on the input information bits based on the calculated reliabilities about them. To reduce the complexity of the inner and outer SISOs, we simulate the max-log versions of them, which are equivalent to modified soft-output VAs (SOVAs) [20]. The simulation results will be given in Subsection VI.E.

### C. Parallel Concatenation

Similar to coded FQPSK in [11–13], we consider a parallel concatenated coding scheme of the turbo-coding type, as illustrated in Fig. 15. In this figure, there is no explicit outer code, but rather the input bits and their interleaved versions are applied to the inherent I- and Q-channel encoders of OQPSK or MIL-STD SOQPSK directly. Therefore, there is no corresponding outer SISO decoder at the receiver. Instead, in each iteration, the output extrinsic information of the I and Q input bits from the inner SISO decoder(s) are fed back as reliabilities of the opposite (I to Q and Q to I) bits after appropriate

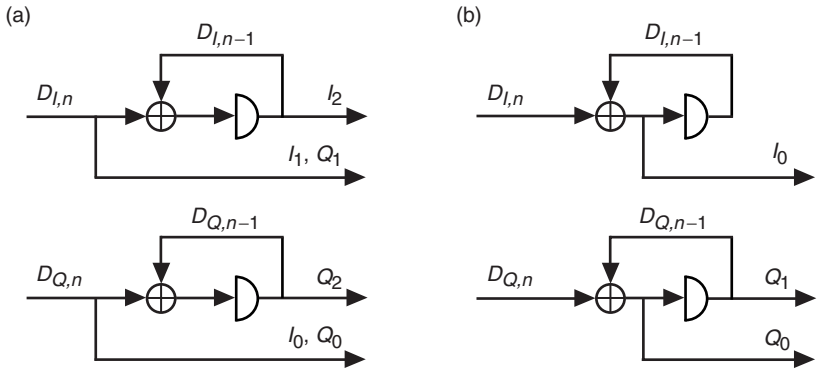


**Fig. 11. Recursive version of the I and Q encoders for: (a) MIL-STD SOQPSK and (b) OQPSK.**

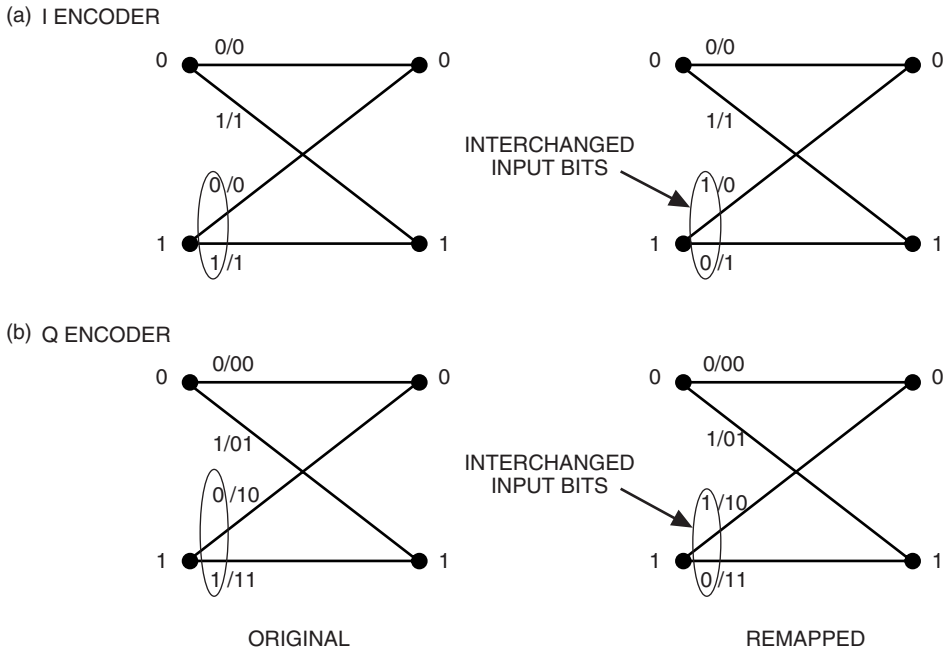


**Fig. 12. Trellis diagrams of the original and remapped (a) I encoder and (b) Q encoder for OQPSK.**

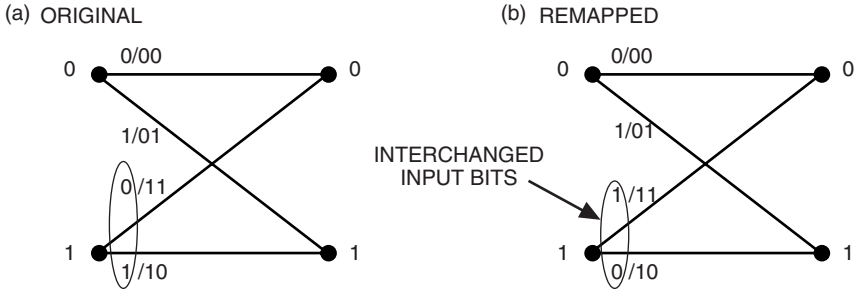


**Fig. 13. Trellis diagrams of the (a) original and (b) remapped I and Q encoders for OQPSK.**

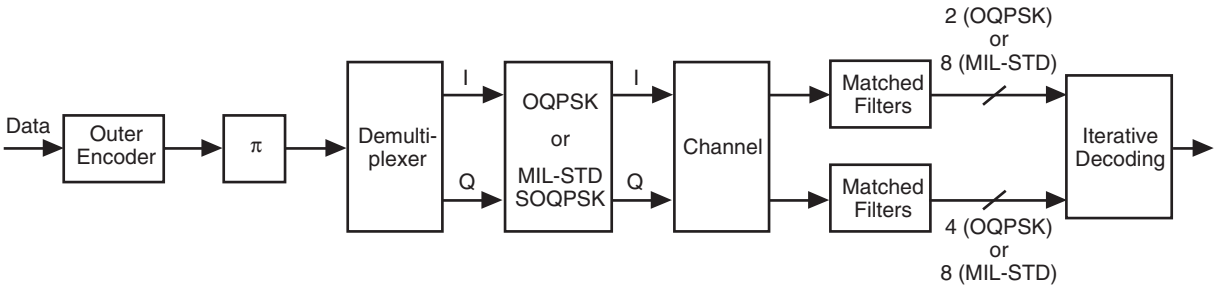


**Fig. 14. Serial concatenated coded system.**

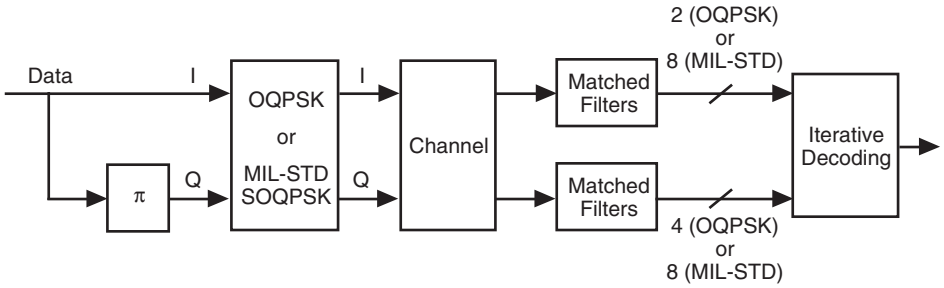


**Fig. 15. Parallel concatenated coded system.**

interleaving and deinterleaving. At the end of the last iteration, the extrinsic information for the I input bits is combined with the deinterleaved extrinsic information for the Q input bits to produce a decision on the input information bits.

### D. Simplified Iterative Decoding for MIL-STD SOQPSK

For both serial and parallel concatenations of coded MIL-STD SOQPSK, it is obvious that the inner SISO decoder for decoding the inherent code of MIL-STD SOQPSK can be replaced with two separate and simplified SISO decoders using the trellis diagrams of the simplified I and Q encoders shown in Fig. 8. Now a joint SISO decoder for decoding the I and Q input bits of the inherent encoder in MIL-STD SOQPSK is not necessary due to the decoupling of the I- and Q-channel transmissions. Consequently, the number of matched filters required in Figs. 14 and 15 can be reduced by half. It will be shown in Subsection VI.E that, although there is a noticeable performance loss due to the simplification, this reduced complexity scheme has a performance comparable to that of coded FQPSK with iterative decoding using the full-blown matched-filter configuration [10] and that it is superior to coded FQPSK with iterative decoding using a simplified receiver [11–13,17].

### E. Simulation Results

In this subsection, we present simulation results for serial and parallel concatenated coded OQPSK and MIL-STD SOQPSK with iterative decoding. Also presented are simulation results of the simplified iterative decoding for MIL-STD SOQPSK as described in Subsection VI.D. In addition, for comparison we have simulated in each case the performance of coded FQPSK with iterative decoding utilizing full-blown matched filters [10] as well as using a simplified receiver structure [11–13,17].

In our simulations, for both the serial and parallel concatenated cases, no termination bits are added anywhere. For serial concatenation, we have investigated two different outer codes. The first one is a rate-1/2 optimum 4-state convolutional code, the recursive structure of which is given in [12]. The second outer code considered is a higher-rate (i.e., 3/4) code obtained from puncturing the first one [12]. Compared to the rate-1/2 code, this code is more bandwidth efficient but less power efficient. In

our simulations, the number of iterations is $L = 5$, and the interleaver block size is $N = 2048$ bits (1024 information bits) for the rate-1/2 outer code. For the rate-3/4 outer code, the interleaver block size is chosen to be $N = 1364$ bits ($1364 \times 3/4 = 1023$ information bits). Note that, for better performance, we have scaled the extrinsic information from the inner SISO(s) and the outer SISO by a factor of 0.75 for the rate-1/2 outer code. For the rate-3/4 outer code, we have scaled the extrinsic information from the inner SISO(s) to the outer SISO by a factor of 0.7, while leaving the extrinsic information from the outer SISO to the inner SISO(s) unchanged. For parallel concatenation, the number of iterations is $L = 8$, and the interleaver block size is $N = 2048$ bits (1024 information bits). In this case, no scaling factor is applied to the extrinsic information from the inner SISO decoder.

Figure 16 shows the BER performances of the three turbo-coded systems with parallel concatenation as well as those of the three serial concatenated coded systems with both the rate-1/2 outer code and the rate-3/4 outer code. From Fig. 16 we see that, for serial concatenation with the rate-1/2 outer code, coded OQPSK has the best performance, as expected, and its performance is very similar to that of serial concatenated coded $\pi/4$-DQPSK with the same rate-1/2 outer code [16]. The performance of coded MIL-STD SOQPSK is only slightly worse than that of coded OQPSK, and it is noticeably better than that of coded FQPSK: at BER $= 10^{-5}$, the required $E_b/N_0$ gap between coded OQPSK and coded MIL-STD SOQPSK is less than 0.02 dB, while it is about 0.09 dB between coded OQPSK and coded FQPSK. The simplified iterative decoding of coded MIL-STD SOQPSK is about 0.1 dB worse than the non-simplified decoding at BER $= 10^{-5}$, and it is very close to that of coded FQPSK with iterative decoding using full-blown matched filters. The simplified decoding of coded FQPSK, however, is about 0.15 dB worse

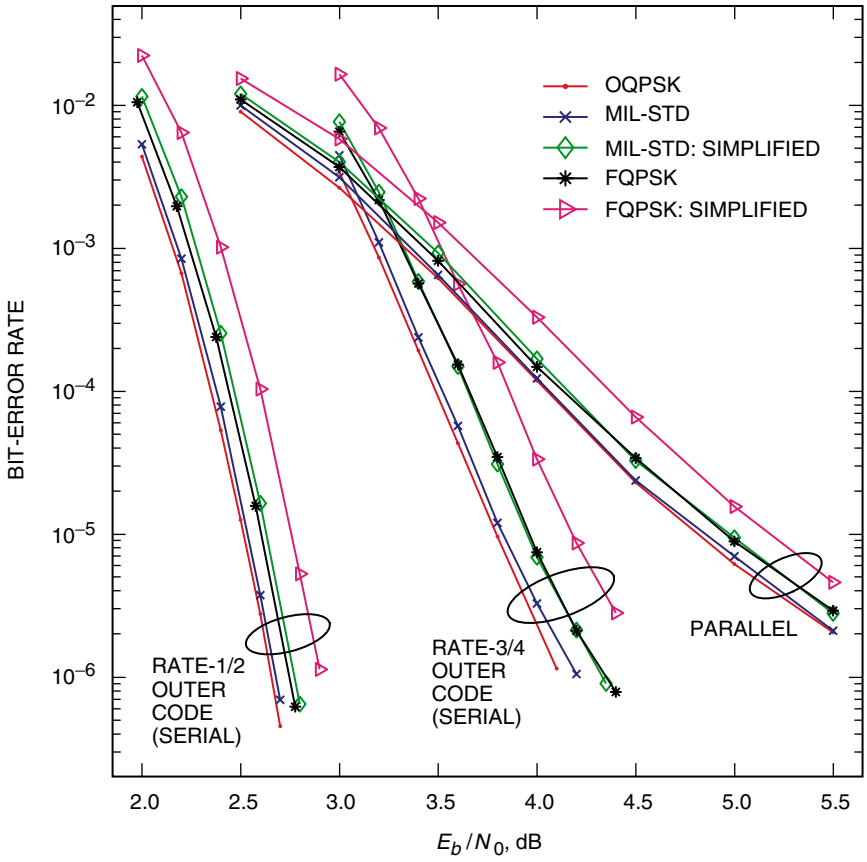


**Fig. 16. BER performance of coded systems with serial and parallel concatenations.**

than the non-simplified decoding at BER $= 10^{-5}$. Compared to the uncoded cases shown in Fig. 10, at BER $= 10^{-5}$, the coding gains for OQPSK, MIL-STD SOQPSK, and FQPSK are 7.05 dB, 7.35 dB, and 7.78 dB, respectively, and the coding gains for the simplified receivers of MIL-STD SOQPSK and FQPSK are 7.43 dB and 7.88 dB, respectively. Therefore, of the three modulation schemes, the more bandwidth efficient a scheme is, the greater is the coding gain.

For serial concatenation with the rate-3/4 outer code, the relations of the five BER curves are very similar to those for the rate-1/2 outer code, except that now the performance of the simplified decoding of coded MIL-STD SOQPSK is almost indistinguishable from that of coded FQPSK. In addition, unlike the rate-1/2 outer code case, the BERs are not decreasing dramatically as $E_b/N_0$ increases, especially at high $E_b/N_0$ ranges. Still, with this rate-3/4 outer code, there are significant coding gains when compared to the uncoded case: at BER $= 10^{-5}$, for OQPSK, MIL-STD SOQPSK, and FQPSK, they are 5.77 dB, 6.03 dB, and 6.41 dB, respectively; and for the simplified decoding of MIL-STD SOQPSK and FQPSK, they are 6.10 dB and 6.45 dB, respectively.

Finally, we observe from Fig. 16 that, with this simple turbo-coding scheme, the relations of the five BER curves are very similar to those of their serial concatenation counterparts, except that now the BERs are decreasing much slower as $E_b/N_0$ increases. In fact, the five BER curves start to show leveling off even before the BER reaches $10^{-6}$. For this simple turbo-coding scheme, when compared to the uncoded systems, the coding gains at BER $= 10^{-5}$ are 4.76 dB, 5.03 dB, and 5.42 dB for OQPSK, MIL-STD SOQPSK, and FQPSK, respectively; and they are 5.08 dB and 5.46 dB for the simplified decoding of MIL-STD SOQPSK and FQPSK, respectively. Although these coding gains are not as big as those obtained with serial concatenation of the same rate convolutional outer code or even the higher-rate (i.e., 3/4) outer code, the iterative decoding complexity of the turbo-coding scheme is much lower than its serial concatenation counterpart due to the lack of need for an outer SISO decoder. Therefore, trade-offs must be made between receiver complexity, coding gain, and bandwidth efficiency when designing coded OQPSK, MIL-STD SOQPSK, and FQPSK systems.

## VII. Conclusions

We have shown that both OQPSK and MIL-STD SOQPSK can be decomposed into a (degraded) trellis encoder and a memoryless mapper. When concatenated with an outer code, coded OQPSK with iterative decoding provides a lower bound to the performance of coded MIL-STD SOQPSK and FQPSK. For MIL-STD SOQPSK, we have analyzed its asymptotic BER performance, presented the optimum receiver structure, and proposed a simplified receiver. The simplified receiver maintains good performance with reduced complexity. Simulation results show that the performance of coded MIL-STD SOQPSK comes very close to that of coded OQPSK and is noticeably better than that of coded FQPSK. When compared to their uncoded systems, there are significant coding gains for both coded OQPSK and MIL-STD SOQPSK applying iterative decoding to either the parallel concatenated coding scheme or the serial one, even when very simple outer codes are used.

## Acknowledgments

The authors would like to thank Dr. Dariush Divsalar and Dennis Lee for many helpful discussions with them.

# References


[1] M. J. Dapper and T. J. Hill, "SBPSK: A Robust Bandwidth-Efficient Modulation for Hard-Limited Channels," *Proc. IEEE Military Commun. Conf. (Milcom'84)*, Los Angeles, California, October 1984.

[2] T. J. Hill, "An Enhanced, Constant Envelope, Interoperable Shaped Offset QPSK (SOQPSK) Waveform for Improved Spectral Efficiency," *Proc. Int. Telemetering Conf. (ITC'00)*, San Diego, California, October 2000.

[3] T. J. Hill, "A Non-Proprietary, Constant Envelope, Variant of Shaped Offset QPSK (SOQPSK) for Improved Spectral Containment and Detection Efficiency," *Proc. IEEE Military Commun. Conf. (Milcom'00)*, Los Angeles, California, October 2000.

[4] P. S. K. Leung and K. Feher, "F-QPSK—A Superior Modulation Technique for Mobile and Personal Communications," *IEEE Trans. Broadcast.*, vol. 39, no. 2, pp. 288–294, June 1993.

[5] M. Geoghegan, "Implementation and Performance Results for Trellis Detection of SOQPSK," *Proc. Int. Telemetering Conf. (ITC'01)*, Las Vegas, Nevada, October 2001.

[6] M. Geoghegan, "Bandwidth and Power Efficiency Trade-Offs of SOQPSK," *Proc. Int. Telemetering Conf. (ITC'02)*, San Diego, California, October 2002.

[7] M. K. Simon and L. Li, "A Cross-Correlated Trellis-Coded Quadrature Modulation Representation of MIL-STD Shaped Offset Quadrature Phase-Shift Keying," *The Interplanetary Network Progress Report 42-154, April–June 2003*, Jet Propulsion Laboratory, Pasadena, California, pp. 1–16, August 15, 2003.
http://ipnpr.jpl.nasa.gov/tmo/progress_report/42-154/154J.pdf

[8] M. K. Simon and T.-Y. Yan, "Cross-Correlated Trellis-Coded Quadrature Modulation," U.S. patent filed, October 1999.

[9] M. K. Simon and T.-Y. Yan, "Performance Evaluation and Interpretation of Unfiltered Feher-Patented Quadrature-Phase-Shift Keying (FQPSK)," *The Telecommunications and Mission Operations Progress Report 42-137, January–March 1999*, Jet Propulsion Laboratory, Pasadena, California, pp. 1–29, May 15, 1999.
http://tmo.jpl.nasa.gov/tmo/progress_report/42-137/137C.pdf

[10] M. K. Simon and T.-Y. Yan, "Unfiltering Feher-Patented Quadrature Phase-Shift-Keying (FQPSK): Another Interpretation and Further Enhancements: Parts 1,2," *Applied Microwave & Wireless Magazine*, vol. 12, nos. 2/3, pp. 76–96/100–105, February/March 2000.

[11] M. K. Simon and D. Divsalar, "A Reduced-Complexity, Highly Power-/Bandwidth-Efficient Coded Feher-Patented Quadrature-Phase-Shift-Keying System with Iterative Decoding," *The Telecommunications and Mission Operations Progress Report 42-145, January–March 2001*, Jet Propulsion Laboratory, Pasadena, California, pp. 1–17, May 15, 2001.
http://tmo.jpl.nasa.gov/tmo/progress_report/42-145/145A.pdf

[12] M. K. Simon and D. Divsalar, "Further Results on a Reduced-Complexity, Highly Power-/Bandwidth-Efficient Coded Feher-Patented Quadrature-Phase-Shift-Keying System with Iterative Decoding," *The Interplanetary Network Progress Report 42-146, April–June 2001*, Jet Propulsion Laboratory, Pasadena, California, pp. 1–7, August 15, 2001.
http://ipnpr.jpl.nasa.gov/tmo/progress_report/42-146/146I.pdf

[13] M. K. Simon and D. Divsalar, "A Reduced Complexity Highly Power/Bandwidth Efficient Coded FQPSK System with Iterative Decoding," *Proc. IEEE Int. Conf. Commun. (ICC'01)*, vol. 7, pp. 2204–2210, Helsinki, Finland, June 2001.

[14] M. Peleg and S. Shamai, "Iterative Decoding of Coded and Interleaved Noncoherent Multiple Symbol Detected DPSK," *Electron. Lett.*, vol. 33, no. 12, pp. 1018–1020, June 1997.

[15] P. Hoeher and J. Lodge, "'Turbo DPSK': Iterative Differential PSK Demodulation and Channel Decoding," *IEEE Trans. Commun.*, vol. 47, no. 6, pp. 837–843, June 1999.

[16] K. R. Narayanan and G. L. Stüber, "A Serial Concatenation Approach to Iterative Demodulation and Decoding," *IEEE Trans. Commun.*, vol. 47, no. 7, pp. 956–961, July 1999.

[17] D. Lee, M. K. Simon, and T.-Y. Yan, "Enhanced Performance of FQPSK-B Receiver Based on Trellis-Coded Viterbi Demodulation," *Proc. Int. Telemetering Conf. (ITC'00)*, San Diego, California, October 2000.

[18] M. K. Simon, *Bandwidth-Efficient Digital Modulation with Application to Deep-Space Communication*, New York: John Wiley & Sons, Inc., 2003, also published as part of the JPL DESCANSO Monograph Series, JPL Publication 00-17, Jet Propulsion Laboratory, Pasadena, California, June 2001.

[19] J. B. Anderson, *Digital Phase Modulation*, New York: Plenum Press, pp. 26–27, 1986.

[20] M. P. C. Fossorier, F. Burkert, S. Lin, and J. Hagenauer, "On the Equivalence between SOVA and max-log-MAP Decodings," *IEEE Commun. Lett.*, vol. 2, no. 5, pp. 137–139, May 1998.